Scientific
Research

A Study on the Conducted Interference of Capacitor Charging Power Supply

Xiao Han[1], Yinghui Gao[2,3], Yaohong Sun[2,3], Ping Yan[2,3]
[1]University of Chinese Academy of Sciences, Beijing, China
[2]Institute of Electrical Engineering, Chinese Academy of Sciences, Beijing, China
[3]Key Laboratory of Power Electronics and Electric Drive, CAS, Beijing, China
Email: hanxiao@mail.iee.ac.cn, gyh@mail.iee.ac.cn, yhsun@mail.iee.ac.cn, pingyan@mail.iee.ac.cn

ABSTRACT

In this paper, a mathematical analysis of the EMI (Electromagnetic Interference) for a 20 kHz/10 kV capacitor charging power supply in frequency-domain is presented, and a related circuit model considering the transient switching interference is proposed. Due to the high working frequency and the device-switching transitions, the conducted EMI caused by the charging circuit which includes the harmonics of grid frequency, working frequency and device-switching transition frequencies. Thus under certain working situations or loads parallel power supply, the interference may cause charging failure. To solve this problem, a high frequency transformer modeled with stray capacitances and an approximation of the device-switching transition is applied in the Spice-based simulation model, and a mathematical analysis in frequency-domain is presented.

Keywords: Capacitor Charging Power Supply; Electromagnetic Transient; Distributed Parameter Circuits; High Frequency and High Voltage Transformer; Frequency Domain Analysis

1. Introduction

The capacitor charging power supply (CCPS) is an important power charging means for industrial and military applications such as distribution energy storage in capacitors. And because increasing the switching frequency is a common manner to obtain high power density, which means shorter transition time during turn-on and off for semiconductor devices and leads to greater high-frequency interference. Moreover, the compact structure of high power density CCPS complicates stray parameters, which cannot be ignored in high-frequency domain. Therefore, the conducted EMI (Electromagnetic Interference) in high power density CCPS is exacerbated and it often causes charging failure under certain working situations or loads such as parallel power supply.

Most of the present models for CCPS do not take into account of the transient switching interference, and the stray parameter obtaining methods are complicated [1]. Furthermore, the mathematical analysis of EMI in frequency-domain is insufficient.

In this paper, analysis of the power supply operation process was conducted and afterwards the required nonlinear elements were modeled, mainly considering the stray parameters in high frequency transformer and the interference of the transient switching harmonics. Satisfactory simulation results which agree with experimental data in frequency domain were obtained. Consequently, the study of the EMI in CCPS can improve its performance and provide guidelines for further power supply design of higher power density.

2. The CCPS Operation Process

Figure 1 shows the configuration for the main circuit of a series resonant capacitor charging power supply (CCPS), which includes a three-phase rectifier, an inverter with high switching frequency, a transformer to boost voltage and a full wave bridge rectification which provide the charging DC output for load. Moreover, switching loss is decreased by a series resonant circuit connected to the inverter with zero current switching-off.
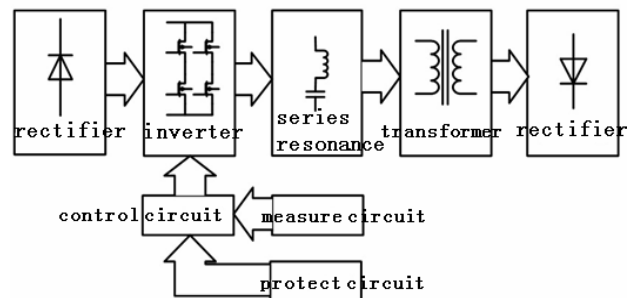
Figure 1. Main circuit of a CCPS.

The grid power is converted by the 3-phase rectifier to a DC voltage supply, and the switching frequency f_s of IGBTs in inverter should be coordinated with the resonance frequency f_r in series circuit as Equation (1).

$$2f_s = f_r \qquad (1)$$

During one switching period, the output current in resonant series circuit flows through one set of IGBTs and corresponding anti-parallel diodes in the first half cycle, and then through the other set. The resonant output current oscillates to zero exactly when the next set of IGBTs switch on due to Equation (1), achieving zero current switching.

Afterwards, the resonant output current charges the capacitor through a high frequency step-up transformer and a full-wave rectifier. The charging current wave in each resonant period is similar during the charging process, which means the average charging current level remains constant. According to Equation (2), the increase in capacitor voltage in each stage is constant, which can be seen approximately as linear.

$$i_c = C \cdot du_c / dt. \qquad (2)$$

3. Mathematical Analysis

Analyze the operation waveform in the charging power supply according to the operation process described before, emphasizing on the resonant output current.

3.1. Circuit of 3-phase Rectifier Filtered by a Capacitor

The 3-phase rectifier filtered by a capacitor is shown in **Figure 2**, in which C is the equivalence of the filter capacitor and load, and L_s, R for stray parameters in load.

The DC output current i_d remains continuous when $\omega RC < \sqrt{3}$, and turns discontinuous when $\omega RC > \sqrt{3}$ [3]. The output current i_d and output voltage u_d under different sets of ωRC are shown in **Figure 3**.

3.2. The Circuit of Inverter

According to 3.1, the DC output voltage of 3-phase rectifier filtered by a capacitor, which supplies for inverter circuit, contains harmonics of $6k(k = 1, 2, 3, \cdots)$, i.e. pulses at a frequency of $6 \times 50 \, \text{Hz} = 300 \, \text{Hz}$. The pulse frequency of the DC supply voltage for inverter is much larger than the switching frequency or resonance frequency, thus the DC supply voltage can be considered as constant when analyzing the inverter waveforms.

During one resonant period $0 \sim T_r$, a set of IGBTs (Q2,Q3) switches on at $t = 0$, and the corresponding anti-parallel diodes(D2,D3) serve as FWD after half cycle, as shown in **Figure 4**.
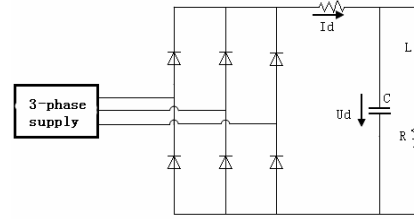
Figure 2. Circuit of 3-phase rectifier filtered by a capacitor.
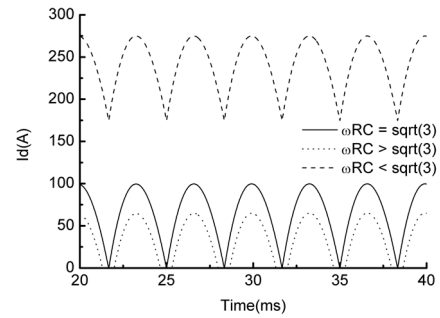
(a)
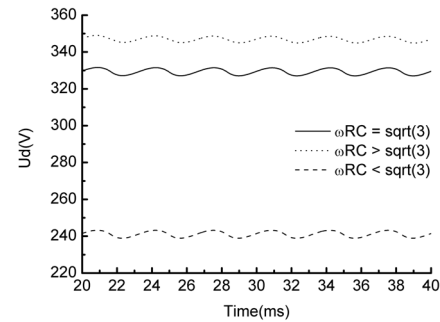
(b)

Figure 3. (a) Output DC current under different conditions; (b) Output DC voltage under different conditions.
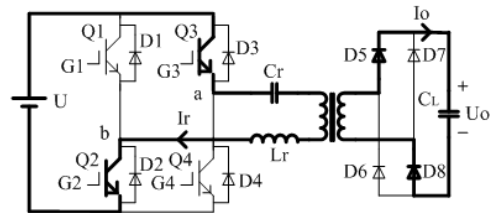
(a)
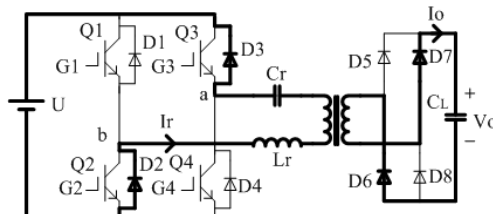
(b)

Figure 4. (a) 0~T_r/2, current flows in IGBTs; (b) T_r/2~T_r, current flows in diodes.

Figure 4 can be simplified into **Figure 5**, and Equations (3)-(6) are listed according to **Figure 5**.

$$i_r = Cr \frac{du_2}{dt} = C_{oe} \frac{du_3}{dt} \qquad (3)$$

$$u_4 = L_r \frac{di}{dt} \qquad (4)$$

$$u_1 = iR \qquad (5)$$

$$U = u_1 + u_2 + u_3 + u_4 \qquad (6)$$

where in $C_{oe} = N^2 C_o \gg C_r$, and since the circuit works under the condition of zero current switching-on and -off, the resonant current can be deduced as Equation (7).

$$i(t) = A \exp(-\alpha t) \sin(\omega_d t) \qquad (7)$$

Equation (7) shows that the resonant output current is in under-damping oscillation form ($R < 2\sqrt{L_r/C_r}$). Set $f_r = \omega_r/2\pi = 1/T_r$ ($\omega_r = \sqrt{1/L_r C_r}$) as the ideal resonance frequency, $f_s = 1/T_s \approx f_r/2$ as the switching frequency, $\alpha = R/2L_r$ as the damping coefficient, and $\omega_d = \sqrt{\omega_r^2 - \alpha^2}$ the real resonance frequency.

During $t = 0 \sim T_r$, set the amplitude of peak point as A_1, A_2, which occur separately at $t_1, t_2 (t_1 < t_2)$. Differentiate Equation (7), and Equations (8)-(9) can be deduced.

$$i(t)' = -A\alpha e^{-\alpha t} \sin(\omega_r t) + A e^{-\alpha t} \omega_r \cos(\omega_r t) \qquad (8)$$

$$i(t_{1,2})' = 0 \qquad (9)$$

Thus the damping coefficient α can be calculated by Equation (10).

$$\alpha = 2\ln\left|\frac{A_2}{A_1}\right|/T_r = 2\ln\left|\frac{A_2}{A_1}\right| f_r \qquad (10)$$

(a)

(b)
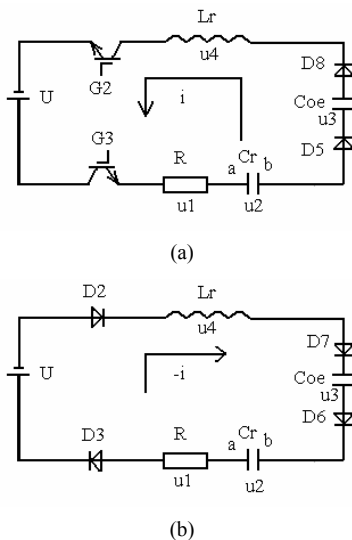
Figure 5(a). 0~T_r/2, current flows in IGBTs; (b). T_r/2~T_r, current flows in diodes.

The experimental data shows that $A_1 = 200\,A$, $A_2 = 90\,A$, and the equivalent series resistor for the testing power supply is $R = 1.7\,\Omega$ by applying Equation (10).

4. Modeling of the Non-linear Element

There are two types of non-linear elements in the CCPS under discussion; the high-frequency transformer and the semiconductor switching devices.

4.1. High Frequency and High Voltage Transformer

The effect of stray parameters, especially stray capacitance under high-frequency working condition, in the transformer cannot be ignored. The two-winding transformer model shown in **Figure 6** is applicable for engineering analysis, where L_{s1}, R_1, C_{10} and L_{s2}, R_2, C_{20} are the leakage inductances, resistances and self-apacitances of the primary, secondary windings, and L_m, R_m and C_{120} respectively refer to the magnetic inductance, equivalent core loss resistance and mutual capacitance between the two windings [4].

The circuit shown in **Figure 6** can be simplified to a two-port network [5-7], as shown in **Figure 7**.

The three parameters in **Figure 7** are related to parameters in **Figure 6** as Equations (11)-(14).

$$C_1 = C_{10} + (1-n)C_{120} \qquad (11)$$

$$C_2 = n^2 C_{20} + n(1-n)C_{120} \qquad (12)$$

$$C_s \approx C_1 + C_2 \qquad (13)$$

$$L_s \approx L_{s1} + \frac{L_{s2}}{n^2} \qquad (14)$$

Under different open- and short-circuit circumstances, the input impedance equations are shown in **Table 1** [6].

The numerical solutions of the related parameters for transformer in the test power supply are $L_s = 12.57\,\mu H$, $L_m = 6\,mH$, $C_s = 5\,nF$.
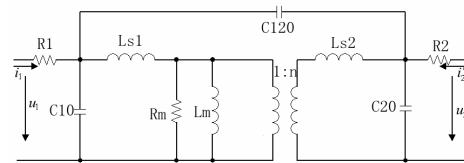
Figure 6. Equivalent circuit of a two-winding transformer.
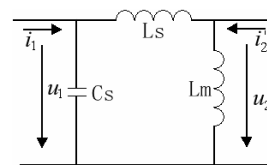
Figure 7. Simplified two-port network of a two-winding transformer.

The ideal part of transformer could be modeled utilizing linear controlled source as illustrated in **Figure 8**, and the whole transformer model can be obtained when combined with the stray parameters.

4.2. Semiconductor Switching Devices

The semiconductor elements contained in the power supply includes power diodes in the three-phase rectifier, IGBTs with anti-parallel diodes in the inverter and diodes in the full wave bridge rectification. All these semiconductor elements can be modeled by utilizing the Model Editor in Cadence Pspice accessories, and the characteristic parameters or curves can be obtained directly from datasheet or measured.

Actually all the semiconductors can be simulated with ideal model except for the anti-parallel diodes in inverter, the reverse recovery process of which cause interference during the circuit changing period, as shown in **Figure 9**, $t_2 \sim t_3$.

Considering the simulation precision and convergence, a sub-circuit Spice model could be applied in simulating the RR process of anti-parallel diodes [8], as principally sketched in **Figure 10**.
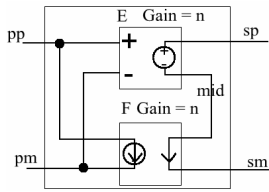
Figure 8. Ideal part of the transformer.
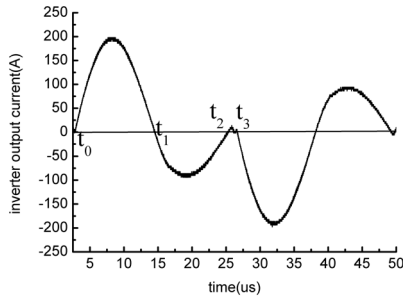
Figure 9. Experimental curve of output current in resonant series circuit.
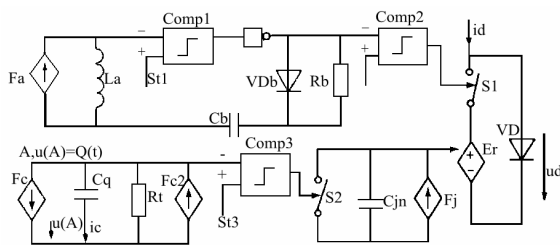
Figure 10. The sub-circuit model of anti-parallel diode.

The testing power supply used FF300R12KS4 module for inverter part, and the parameters of anti-parallel diode can be obtained by its datasheet ($\tau_r = 15$ ns, $\tau_f = 60$ ns, $C_{jn} = 1$ p. The parameters of diode VD for simulating for- ward impedance are $IS = 0.0894$, $N = 2.1822$, $RS = 0.0021$, $IKF = 2.1377e-5$) [9].

5. Simulation Results and Analysis

5.1. Simulation Results

The simulation results agree in acceptable accuracy with the experimental data by applying the models discussed before. **Figure 11** shows the simulated reverse current under different sets of resonance impedance $Z_0 = \sqrt{L_r/C_r}$ for the resonant series circuit, it can be specified that when the resonance impedance decreases, the peak reverse current and the reverse recovery time increases, which generally results in larger ripple components.

5.2. Frequency Domain Analysis

Deduce the frequency spectrum envelope by applying the Fourier differential invariants Equations (15)-(16), which corresponds to the 0dB/dec and $-20n$dB/dec respectively [10].

$$F(\omega) \le \int |f(t)dt| \qquad (15)$$

$$F(\omega) \le \frac{\int |f^{(n)}(t)dt|}{\omega^n} \qquad (16)$$

Substitute Equations (15)-(16) in Equation (7), in which $n = 1$ in Equation (16), and Equations (17)-(18) respectively for 0dB/dec and -20dB/dec are obtained, and the intersection point is the turning frequency.

$$F_1(f) = \int_0^{T_r} |i(t)| dt = A \frac{\omega_r}{\alpha^2 + \omega_r^2}(e^{-\alpha T_r/2} + 1)^2 \qquad (17)$$

$$F_2(f) = \int_0^{T_r} \frac{|i'(t)|}{\omega} dt = \frac{2A}{\omega} \frac{\omega_r e^{-\alpha t_1}}{\sqrt{\omega_r^2 + \alpha^2}}(1 + e^{-\alpha T_r/2}) \qquad (18)$$

Sequentially, other turning frequency points can be calculated in this way. The current harmonics drastically decay at $f \approx f_r = 40$ kHz for the testing power supply.

The reverse recovery current ripple can be handled as a triangular wave whose rising time τ_r and falling time τ_f are determined by the diode essential features and the external parameter resonance impedance Z_0, as explained in 5.1. And the spectrum envelope turning frequency point of the ripple is verified by Equation (19).

$$f_{\text{turning}} = 1/2\pi\tau_r + 1/2\pi\tau_f \qquad (19)$$

The calculating result for testing power supply is $f = 0.8$ MHz with the utilization of experimental data.

Figure 12 shows the spectrum envelope of simulated
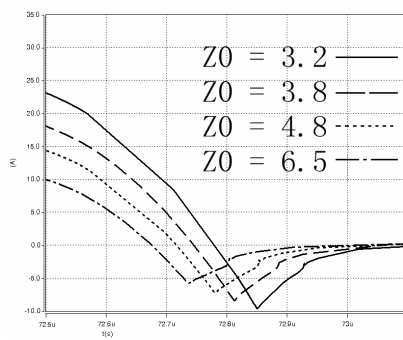
Figure 11. Simulated reverse current under different sets of resonance impedance.
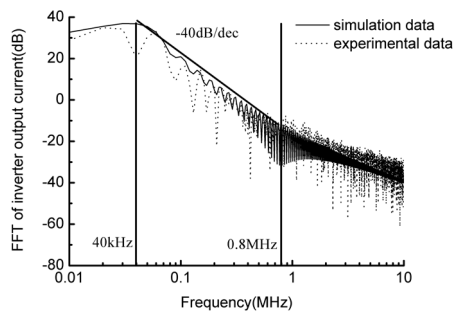
Figure 12. The Bode diagram of output charging current comparing experimental results and simulation results. The two curves agree at harmonic interference points in 20kHz related range and super-0.8MHz range, the former caused by switching frequency and the latter caused by transient switching interference.

output charging current, it is in accordance at most frequencies compared with the experimental data.

6. Conclusions

In this paper, a circuit model considering the transient switching interference for a 20 kHz/10 kV capacitor charging power supply is proposed, in which the stray parameters of high-frequency transformer are numerically solved and an approximation of the device-switching transition are presented. Then the circuit model is analyzed in frequency domain and compared with the experimental data. Afterwards, further details can be provided for the realization of EMI reduction in high frequency and high voltage capacitor charging power supply.

REFERENCES

[1]   W. L. Zhang, "Investigation on Switching Power Supply with High Voltage and High Power (M.S., Graduate school," Chinese Academy of Sciences, Beijing, China, 2003.

[2]   D. Xing, "Development of the 50 kHz Capacitor Charging Power Supply using Series Resonant Topology (M.S., Graduate School," Chinese Academy of Sciences, Beijing, China, 2010.

[3]   Z. A. Wang and J. Huang, "Power Electronics," 4th Edition, China: Machine Press, 2002.

[4]   J. Biernacki and D. Czarkowski, "High Frequency Transformer Modeling," ISCAS 2001: Sydney, Australia, 2001, pp. 676-679.

[5]   Y. A. Wang, "Study of A High Power Frequency Voltage Switch Supply and Monitor System for Electrostatic Precipitator (ESP) Use," Ph.D., Shanghai Jiao Tong University, China, 2010.

[6]   H. Y. Lu, J. G. Zhu and S. Y. R. Hui, "Experimental Determination of Stray Capacitances in High Frequency Transformers," *IEEE Transactions.*

[7]   Z. Y. Zhao, H. H. Qin and C. Y. Gong, "Influences and Suppression Method of Transformer Winding Capacitance in High-frenquency High-voltage Flyback Converter," *Advanced Technology of Electrical Engineering and Energy*, No. 4, 2006, pp. 67-70.

[8]   Y. C. Liang and V. J. Gosbell, "Diode Forward and Reverse Recovery Model for Power Electronic SPICE Simulations," *IEEE Transactions on Power Electronics*, Vol. 5, No. 3, 1990, pp. 346-356.

[9]   L. Z. Yao, "General Circuit Simulation Technology and Software Applications: Spice and Pspice," Beijing: Publishing House of Electronics Industry, 1994.

[10] W. M. Ma, L. Zhang and J. Meng, "Electromagnetic Compatibility of Independent Power System and Power Electronics Device," 1st ed., Science Press, Beijing, 2007.